Atmos. Meas. Tech. Discuss., doi:10.5194/amt-2016-134, 2016
Manuscript under review for journal Atmos. Meas. Tech.
Published: 7 July 2016

Atmospheric Measurement Techniques Discussions

Improvement of Vertical Velocity Statistics Measured by a Doppler Lidar through Comparison with Sonic Anemometer Observations

Timothy A. Bonin[1,*], Jennifer F. Newman[1,+], Petra M. Klein[1,2], Phillip B. Chilson[1,3], and Sonia Wharton[4]

[1]School of Meteorology, University of Oklahoma, Norman, OK, USA
[2]Cooperative Institute for Mesoscale Meteorological Studies, University of Oklahoma, Norman, Oklahoma, USA
[3]Advanced Radar Research Center and School of Meteorology, University of Oklahoma, Norman, Oklahoma, USA
[4]Lawrence Livermore National Laboratory, Livermore, California, USA
[*]Current affiliation: Cooperative Institute for Research in the Environmental Sciences, University of Colorado, Boulder, CO, USA
[+]Current affiliation: National Wind Technology Center, National Renewable Energy Laboratory, Golden, CO, USA

Correspondence to: Timothy A. Bonin (timothy.bonin@noaa.gov)

Abstract. Since turbulence measurements from Doppler lidars are being increasingly used within wind energy and boundary-layer meteorology, it is important to assess and improve the accuracy of these observations. While turbulent quantities are measured by Doppler lidars in several different ways, the simplest and most frequently used statistic is vertical velocity variance (σ_w^2) from zenith stares. However, the competing effects of signal noise and resolution volume limitations, which respectively increase and decrease σ_w^2, reduce the accuracy of these measurements. Herein, an established method that utilizes the autocovariance of the signal to remove noise is evaluated and its skill in also correcting for volume-averaging effects in the calculation of σ_w^2 is assessed. Additionally, this autocovariance technique is further refined by defining the amount of lag time to use for the most accurate estimates of σ_w^2. Through comparison of observations from two Doppler lidars and sonic anemometers on a 300-m tower, the autocovariance technique is shown to improve estimates of σ_w^2 over a variety of atmospheric conditions. After the autocoviance technique is applied, values of σ_w^2 from the Doppler lidars are generally in close agreement ($R^2 \approx 0.95 - 0.98$) with those calculated from sonic anemometer measurements.

1 Introduction

Various scanning strategies and measurement methods have been used to quantify turbulence characteristics from Doppler lidar (DL) observations. Sathe and Mann (2013) summarize the state-of-the-art DL turbulence measurement techniques and limitations with current observations, several of which are briefly described here. One method involves velocity structure functions, which can be calculated longitudinally along the beam or transversely across azimuths in sector plan position indicator (PPI) scans (e.g., Eberhard et al., 1989; Frehlich and Cornman, 2002; Krishnamurthy et al., 2011; Davies et al., 2004). Values of the horizontal wind variance (σ_u^2 and σ_v^2) can be calculated from range height indicator scans, by first separating the measured velocity into height bins and calculating the variance in velocity at each height (e.g., Banta et al., 2006; Pichugina et al., 2008). A novel six-beam technique proposed by Sathe et al. (2015) can be used to calculate all six terms within the Reynolds stress tensor.

Atmos. Meas. Tech. Discuss., doi:10.5194/amt-2016-134, 2016
Manuscript under review for journal Atmos. Meas. Tech.
Published: 7 July 2016

Atmospheric Measurement Techniques Discussions

Quantifying vertical velocity variance σ_w^2 and calculating vertical velocity spectra are some of the simplest and most direct measurements of turbulence that are possible with a DL, since no complex scanning strategies are required and w is being directly measured at high temporal resolution (≈ 1 Hz). These measurements have been used in many studies (e.g., Hogan et al., 2009; Lothon et al., 2009; Barlow et al., 2011; Shukla et al., 2014). For this measurement, the DL simply points at zenith and continually collects measurements of the vertical velocity w, for which σ_w^2, spectra of w, and other turbulence statistics of w can be calculated at every range gate over a user-defined time interval. These measurements are often used to derive other important planetary boundary layer (PBL) variables. Sensible and latent heat fluxes can be retrieved using σ_w^2 and w skewness profiles (Gal-Chen et al., 1992; Davis et al., 2008; Dunbar et al., 2014). The mixing height can be determined from profiles of σ_w^2 as the height where σ_w^2 decreases below a threshold value (Pearson et al., 2010; Barlow et al., 2011). Integral time and length scales, which are critical parameters for turbulence schemes within numerical models, can be calculated from the autocorrelation of w (Lenschow et al., 2000; Lothon et al., 2006). Eddy dissipation rate ϵ can be estimated from the spectrum of w (O'Connor et al., 2010). With all of these above variables being derived from observed fluctuations of w, it is important to assess the accuracy of DL w measurements and their derived statistics.

The mean wind speeds computed from DL velocity-azimuth display (VAD) or Doppler beam swinging (DBS) scans have been shown to compare well to those from anemometers, radiosondes, and radar wind profilers (e.g. Smith et al., 2006). In comparison to sonic anemometers, the sampling volume and averaging time of DLs is large ($\sim$ 20 m and 1 s, respectively), and therefore DLs are unable to resolve smaller scales of turbulence. A diagram showing these effects is provided in Fig. 1. Additionally, DL data can be noisy when aerosol loading and the signal-to-noise ratio (SNR) are small, largely due to limitations in accurately estimating the mean-frequency of the returned signal (e.g. Frehlich and Yadlowsky, 1994). These two limitations have opposite effects on computed higher-order statistics such as σ_w^2. Noise increases computed σ_w^2 and resolution volume effects reduce the values of σ_w^2 measured by the DL compared to the true atmospheric variance. Barlow et al. (2011) compared the standard deviation of w, σ_w, with those from a sonic anemometer and found that the sonic anemometer generally observed larger values of σ_w due to the higher sampling frequency. When the sonic anemometer data were averaged to match the frequency of the DL observations, the values of σ_w from the DL and sonic anemometer were in better agreement, but considerable scatter still existed. Fuertes et al. (2014) used measurements from three synchronous DLs to compute the three-dimensional wind vector at 0.5 Hz for comparison with sonic anemometer measurements, and showed that the DL and sonic measurements were in agreement when the sonic observations were filtered and downsampled to match the spatial and temporal sampling of DL measurements.

Both Barlow et al. (2011) and Fuertes et al. (2014) highlight that DLs are incapable of resolving turbulence on small spatial and temporal scales, as shown in Fig. 1, but do not offer corrections for these limitations in the DL measurements. Hogan et al. (2009) attempts to correct for underestimates of σ_w^2 by extrapolating the power spectrum out to higher frequencies that cannot be resolved by the DL, but does not have sonic anemometer measurements for which these corrected DL σ_w^2 values can be compared. While this method may correct for the inability of DLs to capture smaller scales of turbulence,appropriate techniques for removing noise that can be present in DL observations when SNR is low were not discussed. Herein, we propose to use the autocovariance method discussed by Lenschow et al. (2000) to correct for the effects of both noise and the resolution

Atmos. Meas. Tech. Discuss., doi:10.5194/amt-2016-134, 2016
Manuscript under review for journal Atmos. Meas. Tech.
Published: 7 July 2016

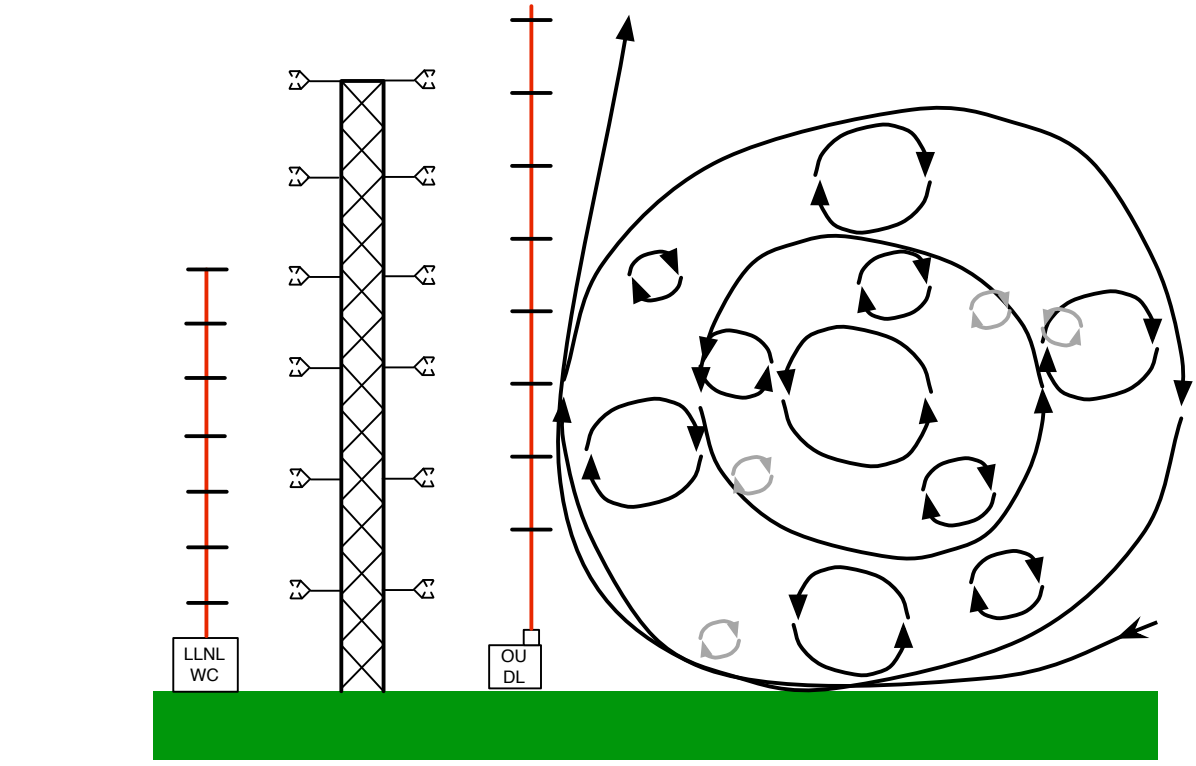

Figure 1. Diagram showing various scales of turbulence compared to the resolution volumes of the DLs and sonic anemometers on the tower. DL beams are denoted by red lines, and range gates by black line segments over it. The DL is able to resolve many of the larger turbulent eddies, but vertical velocities associated with eddies smaller than the range-gate size, such as those shown in grey, cannot be resolved. Many of the smaller eddies may be captured by the sonic anemometer, since their resolution volume is much smaller than the DL. Image is not to scale.

volume to accurately determine the value of variance along the radial velocity; in this case, the analysis focues on measurements when the lidar beam was pointed vertically. Lenschow et al. (2000) originally proposed this method as a means of measuring higher-order moments in noisy data, and the technique will be discussed in detail in Sect. 3.

Few studies compare lidar-derived second- and third-order statistics that utilize the autocovariance method with in situ measurements. Turner et al. (2014a) has compared Raman lidar estimates of water vapour variance and skewness with those from aircraft observations and showed general agreement in the profile shape, but significant differences in the observations were also apparent. Some disagreement in the measurements was partially attributed to sampling differences. Lenschow et al. (2012) compared normalized profiles of DL-derived vertical velocity variance, skewness, and kurtosis with those from other experiments and found generally good agreement. However, to date, the accuracy of these higher-order statistical values from lidars have not been closely evaluated by comparison with other in situ observations.

Atmos. Meas. Tech. Discuss., doi:10.5194/amt-2016-134, 2016
Manuscript under review for journal Atmos. Meas. Tech.
Published: 7 July 2016

Atmospheric Measurement Techniques Discussions

Herein, we provide the first in-depth analysis of the applicability of the autocovariance method of retrieving variance values. DL measurements and derived estimates of σ_w^2 are directly compared with those from sonic anemometers to address the following questions:

1. What are the optimal parameters that should be used when applying the autocovariance method? How sensitive are the derived statistics to these parameters?
2. What scales of turbulence can DLs explicitly resolve? Can the autocovariance technique be used to correct for the limitations of time and volume averaging?
3. How robust are DL-derived estimates of vertical velocity variance, and how does the accuracy of these change with height and for different stability regimes?

A description of the instrumentation used and the experiment, including weather conditions during the measurements, is provided in Sect. 2. The autocovariance technique and the ideal number of lags used in its application is described in detail within Sect. 3. Comparisons of DL and sonic anemometer measurements and derived statistics are presented within Sect. 4. Potential additional applications of this technique and the need for other intercomparison studies are discussed in Sect. 5. A summary and the main conclusions are provided in Sect. 6.

2 Experiment and Instrumentation

Measurements used in this study were collected during the Lower Atmospheric Thermodynamics and Turbulence Experiment (LATTE), which was conducted at the Boulder Atmospheric Observatory (BAO) from 10 February to 28 March 2014 with a small extension to 28 April 2014. The BAO is located 25 km east of the foothills of the Rockies within gently rolling terrain near Erie, CO, USA. The BAO has a suite of permanently and semi-permanently installed meteorological and boundary-layer instruments, such as sodars, a ceilometer, and a 300-m instrumented tower. More complete details of the BAO facility and the surrounding terrain are discussed by Kaimal and Gaynor (1983). In addition to these permanently installed instruments, several Doppler lidars and an unmanned aerial system were deployed at the site by Lawrence Livermore National Laboratory (LLNL) and the University of Oklahoma (OU). Additionally, the National Center for Atmospheric Research (NCAR) deployed a new 449-MHz wind profiler (see Lindseth et al., 2012) at the site for validation of wind and reflectivity measurements.

One of the primary objectives of LATTE was to measure and validate PBL three-dimensional turbulence fields with multiple Doppler lidars, sonic anemometers, an unmanned aerial system, and radar. Several different DL scanning strategies outlined in Sect. 1 were tested for comparison of turbulence measurements with those collected from sonic anemometers. Herein, we focus on measurements taken during a two-day period between 26 March and 28 March, when two DLs were placed within two metres of the sonic anemometer booms on the 300-m tower. Since these measurements are in close proximity with each other, vertical velocity statistics calculated from the DL measurements can be directly compared with those from sonic anemometers. A summary of the instruments used within this study is provided in Table 1, and they are described in more detail below.

Atmos. Meas. Tech. Discuss., doi:10.5194/amt-2016-134, 2016
Manuscript under review for journal Atmos. Meas. Tech.
Published: 7 July 2016

Atmospheric Measurement Techniques Discussions

Table 1. Overview of all instruments and their properties that are used here.

Instrument	Measurement Heights	Sampling Rate	Owner	Boom
R.M. Young 3-D Sonic Anemometers	50, 100, 150, 200, 250, 300 m	30 Hz	OU	North-west
Campbell Scientific CSAT3 3-D Sonic Anemometers	50, 100, 150, 200, 250, 300 m	60 Hz	NCAR	South-east
Halo Streamline Doppler Lidar	99 m–9.6 km 18-m range gates	0.7 Hz	OU	South-east
WindCube v2 Doppler Lidar	40-200 m 12 measurement heights 20-m range gates	0.25 Hz for vertical beam	LLNL	North-west

2.1 Boulder Atmospheric Observatory Tower

The 300-m BAO tower is permanently instrumented with cup anemometers, temperature, humidity, and ozone sensors at 10-, 100-, and 300-m on booms extending to the southeast (154°) of the tower. In addition to these measurements, six sonic anemometers were temporarily installed on booms on both the southeast and northwest (334°) side of the tower. The sonic anemometers were equally spaced every 50-m in height, with the lowest mounted at 50-m and the highest at the top of the tower at 300-m. Six R.M. Young 3-D sonic anemometers (model 81000, R.M. Company, Traverse City, Michigan, USA) provided by OU were installed on the northwest booms, and these sampled at 30 Hz. NCAR provided the Campbell Scientific 3-D sonic anemometers (CSAT 3, Campbell Scientific, Logan, Utah, USA), which sampled at 60 Hz, that were installed on the southeast booms. A spike filter was used to remove erroneous measurements, in which data points that were farther than three standard deviations of the mean, calculated over 30-min windows, were removed.

2.2 Doppler Lidars

Two DLs, a LLNL WindCube v2 (henceforth LLNL WC) and an OU Halo Streamline (henceforth OU DL), were deployed next to the base of the 300-m tower from 26 March to 28 March. The WC was situated to the northwest of the tower, while the OU DL was deployed southeast of the tower. The DLs were located a few metres from the ends of the booms on the tower so that the beam would not be obscured. For the analysis, turbulence statistics from each DL were generally compared with those from the sonic anemometers above each lidar. Specifically, statistics from the LLNL WC are compared with those from the R.M. Young anemometers, and statistics from the OU DL are compared with those from the CSAT 3 anemometers.

Atmos. Meas. Tech. Discuss., doi:10.5194/amt-2016-134, 2016
Manuscript under review for journal Atmos. Meas. Tech.
Published: 7 July 2016

Atmospheric Measurement Techniques Discussions

2.2.1 OU Halo Streamline

The OU DL uses a pulsed, heterodyne 1.5 μm laser to detect backscattered energy from aerosols within the atmosphere and to determine the radial velocities along the laser beams from the Doppler shift in the received signal. The range gate size is user-adjustable, with a minimum spacing of 18-m that was used during this portion of LATTE. The smallest range gate spacing of 18-m was chosen to minimize the effects of volume averaging. The focus was set at 300 m, which is the minimum possible focus length, so that generally the largest SNR and highest-quality data are at that height. Since the aerosol content of the air was generally low during the experiment, as predominantly westerly winds advected clean air from the Rocky Mountains over the BAO site, the noise in the measurements tends to increase significantly for measurements closer to the surface and farther from the focus height. Details about the Halo Streamline hardware, specifications, and theory of operation can be found in Pearson et al. (2009).

2.2.2 LLNL WindCube v2

The LLNL WC was designed primarily for wind energy applications, and thus continuously conducts DBS scans for retrieval of horizontal winds within the lowest 200 m of the atmosphere. The DBS scan consists of consecutive beams off-zenith pointing north, east, south, west, and followed by a vertically pointing beam. The vertical velocity component w is directly measured by the vertical beam and is the only variable from the LLNL WC that is used within this analysis. Independent measurements of w from the vertical beam are available approximately every 4 s. The range gate size is 20 m, which is slightly larger than that for the OU DL. Typically during LATTE, the SNR values from LLNL WC measurements are largest at 50 m and decrease with height; thus the highest-quality measurements are closer to the surface than those from the OU DL.

2.3 Meteorological Conditions

To document the general meteorological conditions, mean temperature, wind speeds, and bulk Richardson number (Ri) at three heights during the two-day period when the DLs were located next to the towers are shown in Fig. 2. The value of Ri, which is used as a proxy for stability, is calculated as

$$\mathrm{Ri} = \frac{\frac{g}{\theta}\frac{\Delta\theta}{\Delta z}}{\frac{V^2}{z^2}}, \tag{1}$$

where g is gravity, θ is the potential temperature, $\Delta\theta$ is the difference in temperatures between the measurement height and that at 10-m, Δz is the difference in sampling heights (i.e, $z - 10$ m), z is height, and V is the wind speed at the height that Ri is calculated, implicitly assuming that the surface wind speed is zero.

During a significant portion of the observational period, the wind speed in the lowest 300-m was greater than 5 m s^{-1}. Particularly high winds occurred around 0300 UTC on 27 March. Since the wind direction was westerly (wind direction not shown), these were likely associated with downsloping flow that frequently occurs in this area on the lee of the mountains, which transports momentum downward from higher in the troposphere (e.g., Brinkmann, 1974). Conditions predominantly

Atmos. Meas. Tech. Discuss., doi:10.5194/amt-2016-134, 2016
Manuscript under review for journal Atmos. Meas. Tech.
Published: 7 July 2016

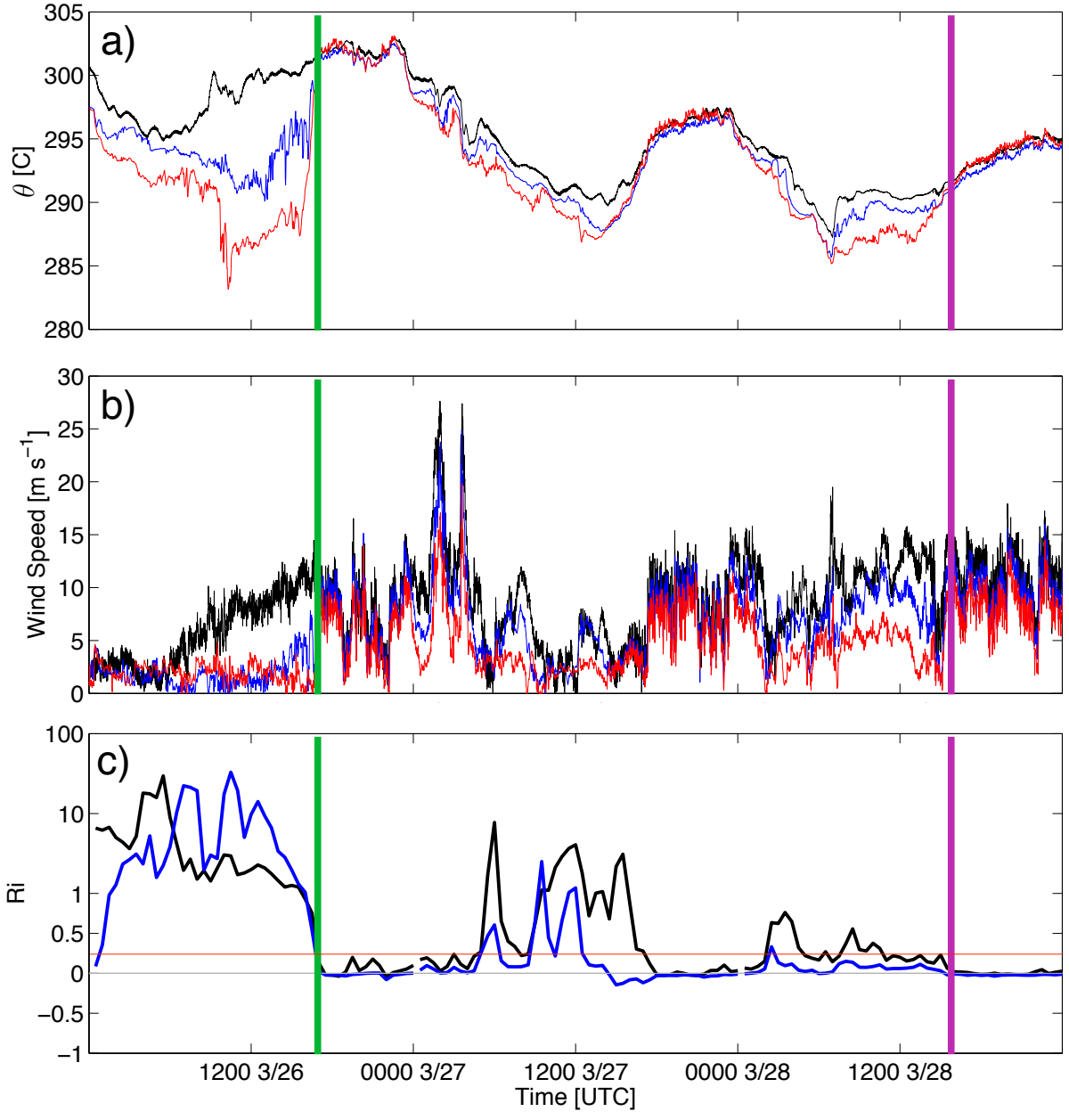

Figure 2. Evolution of θ (a), wind speed (b), and Ri (c) over the two-day observational period from 26 to 28 March, 2014. The colours indicate the height of the measurement on the BAO tower, for which red is 10-m, blue is 100-m, and black is 300-m. Thick green lines denotes when DLs were setup and began operating near the tower, while the magenta lines indicate the end of this observational period. Red horizontal line in (c) shows Ri=0.25 for reference, above which conditions typically are strongly stable and turbulence becomes intermittent.

Atmos. Meas. Tech. Discuss., doi:10.5194/amt-2016-134, 2016
Manuscript under review for journal Atmos. Meas. Tech.
Published: 7 July 2016

Atmospheric Measurement Techniques Discussions

supported neutral stability during the study period. Stable conditions (Ri > 0.25) were observed for several hours on 27 March, but strongly unstable conditions where Ri < -0.1 were never present.

3 Correction of Lidar Variance Values

Lenschow et al. (2000) discusses a methodology of estimating second- through fourth-order moment values within noisy measurements, with a focus on observations taken by various types of lidars. This technique has been used in numerous studies to estimate second- and higher-order moments of water vapour from Raman lidars and Differential Absorption lidars (DIALs) (e.g., Machol et al., 2004; Wulfmeyer et al., 2010; Turner et al., 2014a, b), temperature from Raman lidar (e.g., Behrendt et al., 2015), ozone from a DIAL (e.g., Machol et al., 2009; Alvarez II et al., 2011), velocity from Doppler lidars (e.g. Grund et al., 2001; Tucker et al., 2009), and it was also extended to correct eddy-covariance flux measurements of trace gases (e.g., Mauder et al., 2013; Peltola et al., 2014). While this methodology has been used within many studies, to the authors' knowledge there are no in-depth evaluations of corrected and uncorrected turbulence statistics, using the Lenschow et al. (2000) technique, of any quantity measured by a lidar against in situ observations. Herein, we evaluate the applicability of this technique to extract accurate variance estimates from lidar measurements.

3.1 Overview of Method

The method described by Lenschow et al. (2000) to obtain turbulence statistics in noisy data is outlined here. The second-order autocovariance function (M_{11}) of a stationary time series is defined as

$$M_{11}(t) = \overline{(w' + \epsilon')(w'_t + \epsilon'_t)}, \tag{2}$$

where $w(t)$ is a correlated variable (herein, specifically vertical velocity), ϵ is contamination from random white noise, t is the time-lag, and primes denote deviations from the mean. If the noise is uncorrelated, as is expected with lidar measurements, the cross terms become small and negligible, thus at a lag of zero

$$M_{11}(0) = \overline{w'^2} + \overline{\epsilon'^2}. \tag{3}$$

This relationship shows that the measured variance by the lidar $M_{11}(0)$ is the result of both the true atmospheric variance $\overline{w'^2}$ and the noise variance in the returned signal $\overline{\epsilon'^2}$. By assuming that $\overline{w'^2}$ is largely due to isotropic turbulence within the inertial subrange (Monin and Yaglom, 1979), which is generally true within the PBL except when gravity waves are present, the expected autocovariance function M^*_{11} is

$$M^*_{11}(t) = \overline{w'^2} - Ct^{2/3}, \tag{4}$$

Atmos. Meas. Tech. Discuss., doi:10.5194/amt-2016-134, 2016
Manuscript under review for journal Atmos. Meas. Tech.
Published: 7 July 2016

Atmospheric Measurement Techniques Discussions

in which C is a parameter related to eddy dissipation since w is a component of the velocity. Henceforth, the fitting of Eq. 4 will be referred to as the 'structure function fitting', as the 2/3-power within Eq. 4 ultimately stems from Kolmogorov's structure function (Kolmogorov, 1941). By treating both $\overline{w'^2}$ and C as unknowns and fitting M_{11}^* to the observed M_{11} at lags within the inertial subrange, estimates of $\overline{w'^2}$ and $\overline{\epsilon'^2}$ can be made wherein

$$\overline{w'^2} = M_{11}^*(0) \text{ and} \tag{5}$$

$$\overline{\epsilon'^2} = M_{11}(0) - M_{11}^*(0). \tag{6}$$

Using this relationship implicitly requires that Taylor's frozen hypothesis is valid (Taylor, 1938), meaning that turbulent eddies do not evolve over time as they pass through the resolution volume for time scales over which the fitting of Eq. 5 is applied.

3.2 Number of Lags for Fitting

For the most accurate and robust estimates of variance or higher-order moments, the proper number of lags to use for the fitting is not well-known or trivial. Within many studies in which this method is used, the number of lags used is either not discussed or a seemingly arbitrary number of lags that the authors determined were within the inertial subrange is used (e.g. Lenschow et al., 2000; Wulfmeyer et al., 2010). Previously, the maximum lag time (τ_{max} below) used within the fitting ranges from 12.5 s (e.g., McNicholas and Turner, 2014) to over 100 s (e.g. Behrendt et al., 2015). Ideally, the smallest lag used in the fitting should correspond to the time scale at which contributions to M_{11} from turbulent eddies that cannot be explicitly resolved become negligible. This can also be thought of as the time scale corresponding to the smallest-scale eddies that can be resolved by the lidar. The largest lag to be used should be within the inertial subrange, but not so long that frozen turbulence cannot be safely assumed. The total number of lags used should be enough that an accurate and representative fitting can be ensured.

Here, we define the ideal lags to use in the fitting based on the resolution of the instrument and turbulence characteristics. Since the smallest lag is related to the time scales of the turbulent eddies that cannot be resolved by the lidar, we define the smallest lag τ_{min} to be

$$\tau_{min} = \frac{\Delta r}{V}, \tag{7}$$

where Δr is the size of the range gate or resolution volume and V is the mean horizontal wind speed. Assuming that turbulence is isotropic, this ensures that τ_{min} is large enough that eddies of the same size or smaller than the resolution volume, which lead to underestimates of the true M_{11} at short lags, will not negatively affect the fitting. Within this study, the maximum value of τ_{min} is set to 8 s for time periods when the wind speed is small. This maximum for τ_{min} is somewhat arbitrary, but a maximum value is needed since $\tau_{min} \to \infty$ as $V \to 0$. Since the evolution of turbulent structures becomes significant for larger lag times

Atmos. Meas. Tech. Discuss., doi:10.5194/amt-2016-134, 2016
Manuscript under review for journal Atmos. Meas. Tech.
Published: 7 July 2016

Atmospheric Measurement Techniques Discussions

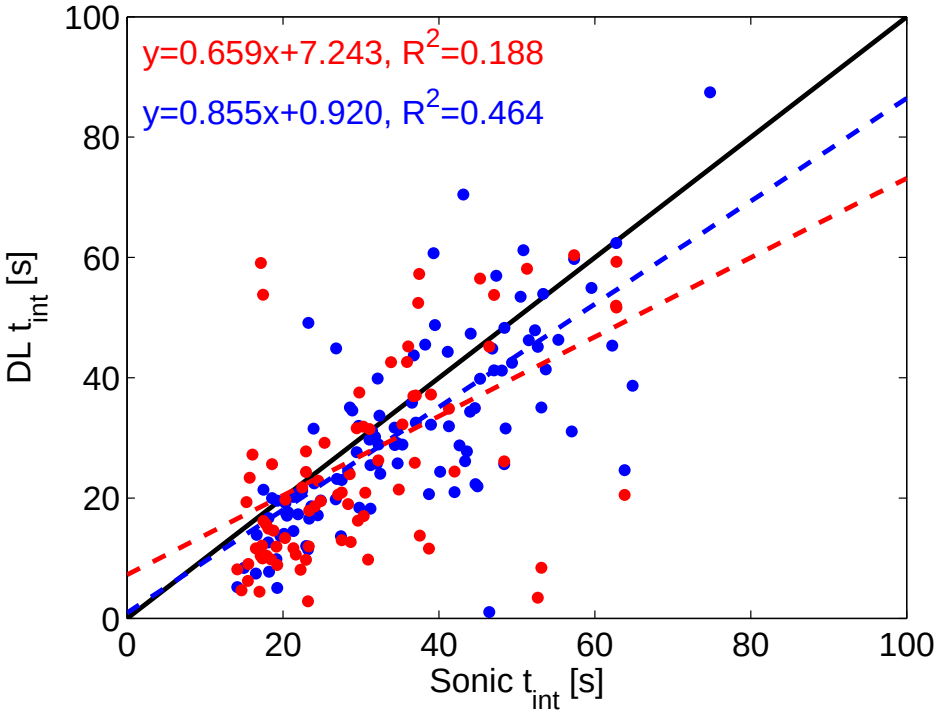

Figure 3. Comparison of t_{int} as calculated from the sonic anemometer and DL M_{11} values, using Eq. 9. Red shows values calculated from LLNL WC measurements, and blue shows those calculated from the OU DL observations. Black solid line shows a one-to-one relationship. The dashed lines show the linear regressions, with the equations for linear regression and coefficients of determination shown in the upper left corner.

(Higgins et al., 2013), this limit for τ_{min} is a compromise between minimizing the effects of both volume averaging and time evolution of turbulence.

We define the largest lag τ_{max} to use as

$$\tau_{max} = \min\left(\frac{t_{int}}{2}, t\left(M_{11}(t) = \frac{M_{11}(0)}{2}\right)\right), \tag{8}$$

where t_{int} is the integral time scale. Under convective conditions, generally $\tau_{max} = \frac{t_{int}}{2}$. However, under more stable conditions, computed values of t_{int} often becomes much larger than the typical time scales within the inertial subrange due to the

Atmos. Meas. Tech. Discuss., doi:10.5194/amt-2016-134, 2016
Manuscript under review for journal Atmos. Meas. Tech.
Published: 7 July 2016

Atmospheric Measurement Techniques Discussions

small value of $\overline{w'^2}$. Under these conditions, the time at which $M_{11} = \frac{M_{11}(0)}{2}$ is used for τ_{max} instead. Values of t_{int} are defined as

$$t_{int} = \frac{1}{\overline{w'^2}} \int_0^{t(M_{11}=0)} M_{11}(t)dt, \tag{9}$$

wherein $\overline{w'^2}$ is $M_{11}^*(0)$, and both t_{int} and $\overline{w'^2}$ are both iteratively solved. Values of t_{int} calculated from the DL observations compared with those calculated from sonic anemometer measurements are shown in Fig. 3. Generally, the values of t_{int} calculated from the OU DL are in better agreement with those derived from anemometer measurements than those from the LLNL WC. This is likely due to the faster sampling rate of the OU DL, therefore the time between lags (dt) is shorter in the numerical integration. Considerable scatter is evident in the estimates of t_{int}, which is due to the differences in the values of M_{11} at various lags that is discussed within Sect. 4.3.

If the conditions are such that τ_{min} is greater than τ_{max}, such as in the stable boundary layer with weak winds, then τ_{max} is set to be one lag more than τ_{min}. Using this method for such time periods when the integral time scale is not explicitly resolved is not ideal since values of M_{11} are not accurately modeled by Eq. 4. However, as shown in Sect. 4.4, this method often improves estimates of σ_w^2 during these time periods by removing noise, which can be significant compared to the small values of σ_w^2. Typical values of τ_{min} and τ_{max} that were used during LATTE are shown in Table 2.

When using the autocorrelation fitting to determine the value of $\overline{w'^2}$ and $\overline{\epsilon'^2}$, it is expected that $M_{11}^*(0)$ (i.e., $\overline{w'^2}$) is less than $M_{11}(0)$, and that $\overline{\epsilon'^2}$ is the positive difference of $M_{11}(0)$ and $\overline{w'^2}$. An example of this is shown in Fig. 4a, where the fitting of Eq. 4 leads to a smaller estimate of $\overline{w'^2}$ than M_{11} at lag zero. However, we observe that under periods of strong turbulence and high SNR, estimates of $\overline{w'^2}$ can be greater than $M_{11}(0)$ as shown in Fig. 4b. Using the definition in Eq. 6, values of $\overline{\epsilon'^2}$ are negative in these cases, which is physically impossible since $\overline{\epsilon'^2}$ in the signal is always positive or zero. To our knowledge, this behaviour has not been discussed in any previous studies. We attribute this 'negative error' to volume-averaging effects, where the smaller scales of turbulence cannot be properly captured by the DL and when the true noise in the measurements is small. This generally occurs when τ_{min} is large (> 4 s), when averaging effects are significant due to the slow advection of eddies through the measurement volume. The accuracy of the fitting under conditions when $M_{11}^*(0)$ is both greater and less than $M_{11}(0)$ is discussed in Sect. 4 through comparison with sonic anemometer measurements.

Table 2. Typical values of τ_{min} and τ_{max} that are used during LATTE.

	Min [s]	Max [s]	Mean [s]	Standard Deviation [s]
τ_{min}	1.4	8	2.9	2.2
τ_{max}	2.8	35	11.5	9.1

Atmos. Meas. Tech. Discuss., doi:10.5194/amt-2016-134, 2016
Manuscript under review for journal Atmos. Meas. Tech.
Published: 7 July 2016

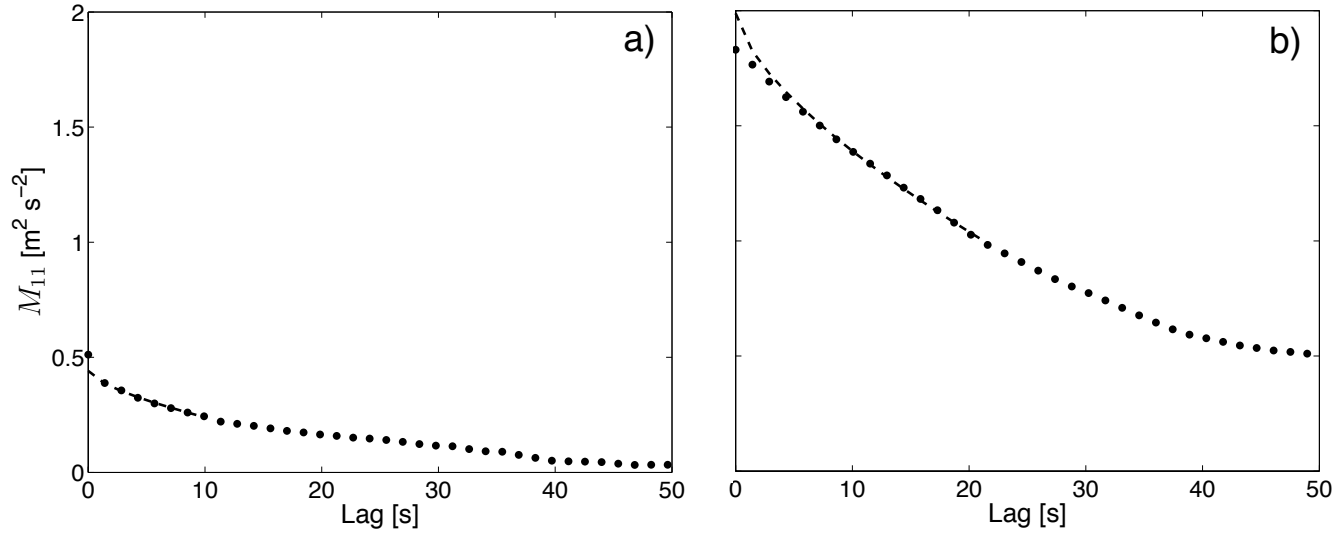

Figure 4. The dashed black lines are example fittings of the structure function (Eq. 4) to M_{11} values from the DL observations, which are shown by black dots. The fitting shown in (a) is expected when white noise is present, as the peak at lag zero is attributed to noise. Within (b), M_{11} at lags zero and one are less than is expected from isotropic turbulence. This is attributed to the volume and time averaging effects of the DL when noise values are very low.

Numerous studies discuss the importance of considering the averaging time when measuring turbulence statistics (e.g. Lenschow et al., 1994; Mahrt, 1998; Hollinger and Richardson, 2005). These errors are related to the representativeness of statistics from a single point measurement to the PBL as a whole, and need to be considered when making generalizations about the PBL from single-point measurements. However, they are outside of the scope of this study. Since measurements from the DL and sonic anemometer were taken within a few metres of each other, which is smaller than the resolution volume of the DL, measured statistics are expected to be very similar to each other and errors due to the spatial separation of the instruments should be minimal. Any differences in statistics of w between the two instruments are more likely due to differences in sizes of sampling volumes and measurement principles.

4 Comparison of Vertical Velocity Statistics

Observations are averaged over 30-min windows for the computation of M_{11} and other vertical velocity statistics from the DLs and sonic anemometers. During time periods when the instruments are waked from the 300-m tower, data are removed since characteristics of the sampled turbulence will be influenced by the tower and not representative of the PBL. To elimate possibly waked measurements, observations are removed when the upwind direction was within $\pm 45°$ of the tower. Measurements are also removed during time periods when precipitation or virga are evident on ceilometer measurements at the BAO site, since precipitation affects the DL measured w. Since the method discussed in Sect. 3 quantifies and removes noise, no explicit SNR

Atmos. Meas. Tech. Discuss., doi:10.5194/amt-2016-134, 2016
Manuscript under review for journal Atmos. Meas. Tech.
Published: 7 July 2016

Atmospheric Measurement Techniques Discussions

filter was used to remove observations. All measurements of w from the DLs, regardless of the SNR value, are used in the computation of σ_w^2. However, DL data are removed during time periods when the estimated $\overline{\epsilon'^2}$ is larger than a threshold. Several different threshold values were evaluated, and a threshold of 1 m^2 s^{-2} was a good compromise between keeping data where accurate σ_w^2 statistics can be retrieved and eliminating meaningless results. Threshold values based on the ratio of $\overline{\epsilon'^2}$ to σ_w^2 were evaluated, but no threshold ratio could be found that both kept accurate values of low σ_w^2 and removed inaccurate values of high σ_w^2. Sampling errors $\Delta\sigma_w^2$, which are errors due sample unrepresentativeness of the population, were calculated using formulations within Lenschow et al. (1994). These errors were found to be less than 5% of σ_w^2 for 84% of all DL observations due to the long half-hourly averaging time in comparison to t_{int} which was typically on the order of 1 min. In fact, for 50% of the DL estimates, the sampling error is less than 1%. Thus, throughout the rest of this study, sampling error is generally not a significant source of error and discrepancy between the DLs and the sonic anemometers, especially since the measurements were taken in such close proximity with each other. If the sonic anemometer and DL were farther apart, these errors would be much more important.

4.1 Effect of Temporal Averaging and Number of Lags for Fitting

As discussed in Sect. 3.2, the proper number of lags to use for the fitting of the Eq. 4 has not been evaluated carefully previously. Here, the autocovariance method is applied using various time lags to identify the accuracy of estimated values of σ_w^2 for differing numbers of lags. Measurements of w from the SE sonic anemometer at 300-m are averaged over 1-s (1-Hz) and 10-s (0.1-Hz) intervals, to simulate the typical averaging times of DLs and DIALs/Raman lidars respectively. From these averaged timeseries, values of M_{11} are calculated to test various lag times for the extrapolation.

Examples of M_{11} calculated from the raw and averaged sonic anemometer measurements are shown in Fig. 5, with fittings of the structure function applied using the specified number of lags outlined in Sect. 3.2. τ_{min} is calculated assuming a range gate size of 20 m, simulating DL values of τ_{min}. Values of $M_{11}(0)$ from the 1-Hz and 0.1-Hz averaged data are smaller than those from the 60-Hz observations, since small-scale fluctuations are removed during the averaging. However, values of M_{11} at larger lags, from the 1-Hz averaged and raw observations, are often very similar. Thus, the fitting of the structure function to the 1-Hz observations generally accurately models M_{11}, and the extrapolation to zero lag is nearly identical to that from the raw time series. Values of M_{11} from the 10-s averaged data are not in good agreement with those from the raw timeseries, especially when M_{11} decreases quickly at small timescales as in Fig. 5a, b. Due to these differences, values of M_{11} are not accurately modeled when fitting the structure function to the 0.1-Hz observations.

To further evaluate the effect of averaging time and amount of lag time used, comparisons of estimates of σ_w^2 using the structure function fitting are compared with those from raw sonic anemometer measurements, shown in Fig. 6. Estimates of σ_w^2 are calculated from the 0.1- and 1-Hz measurements using both 100-s of lag time and the previously defined number of ideal lags. The 100-s of lag time is similar to those used when applying this method to DIAL or Raman lidar measurements (e.g., Behrendt et al., 2015), which is needed since these observations are contaminated by significantly larger values of ϵ'^2 and the sampling rate is much lower.

Atmos. Meas. Tech. Discuss., doi:10.5194/amt-2016-134, 2016
Manuscript under review for journal Atmos. Meas. Tech.
Published: 7 July 2016

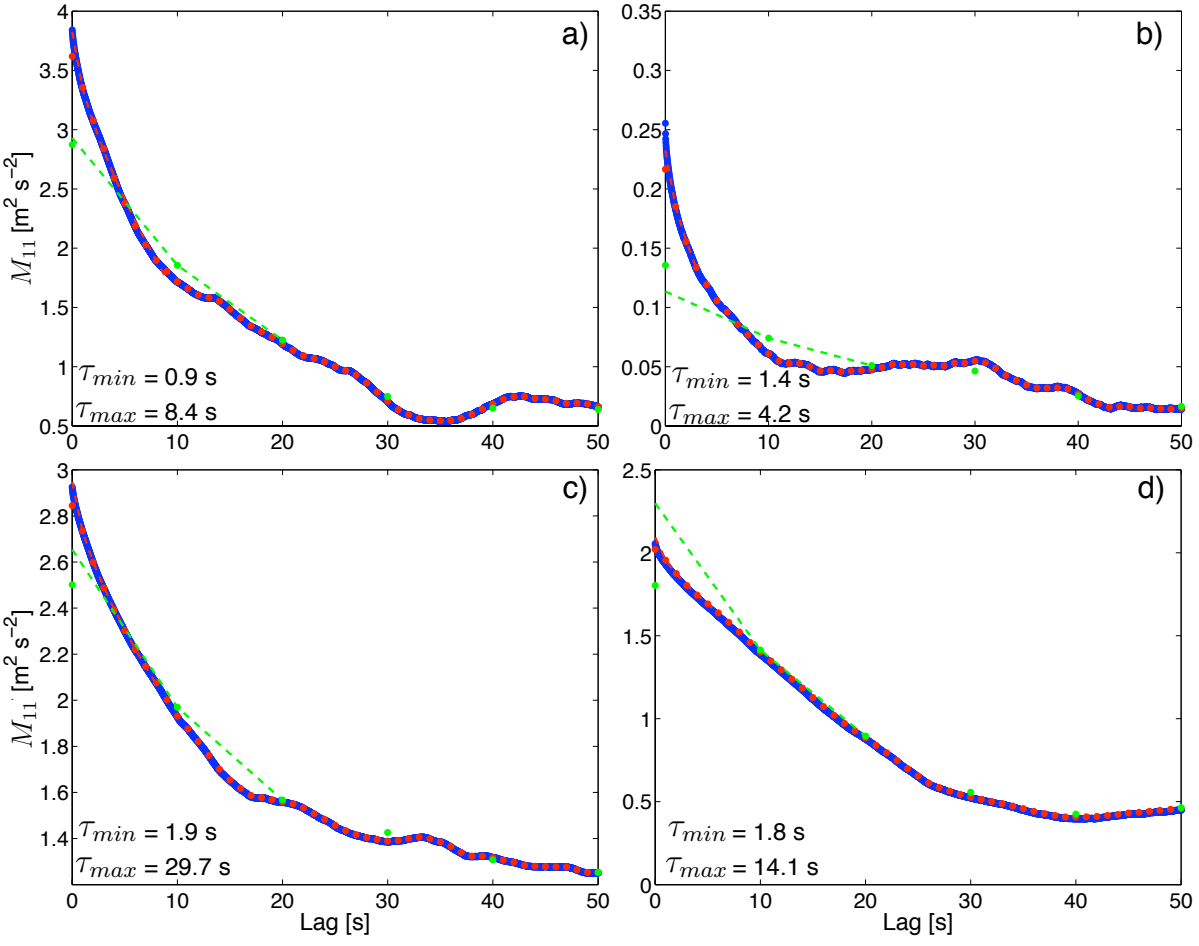

Figure 5. Sample M_{11} from the 300-m 60-Hz sonic data (blue dots) compared with the sonic data averaged to 1-Hz (red dots) and 0.1-Hz (green dots). Dashed lines are the fittings of Eq. 4 to the filtered sonic data, using the specified number of lags discussed in Sect. 3.2. M_{11} is calculated over 0200–0230 UTC (a), 0100–01300 UTC (b), 2000–2030 UTC (c), and 2030–2100 UTC (d) all on 27 March. Values of τ_{min} and τ_{max} are provided in the lower left.

Using the previously mentioned ideal number of lags, the σ_w^2 estimates from the 1-Hz averaged data are in close agreement with those calculated from the raw 60-Hz measurements for the entire range of σ_w^2. This indicates that the sonic observations can be accurately modeled by the structure function fit and contain little noise after the spike removal mentioned in Sect. 2.1. Additionally, the lags defined in Sect. 3.2 are appropriate to use to retrieve accurate estimates of σ_w^2. With the 0.1-Hz averaged observations, estimates of σ_w^2 generally are in agreement with the true value of σ_w^2 when using the appropriate number of lags, although greater scatter is apparent. This also shows that the random error that may arise from using varying numbers of lags, rather than a set number of lags, is minimal. If the random error were to change drastically based on the variable number of lags used in the fitting, there would be much larger scatter for some of the data points depending on the amount of lags that are used.

Atmos. Meas. Tech. Discuss., doi:10.5194/amt-2016-134, 2016
Manuscript under review for journal Atmos. Meas. Tech.
Published: 7 July 2016

Atmospheric Measurement Techniques Discussions

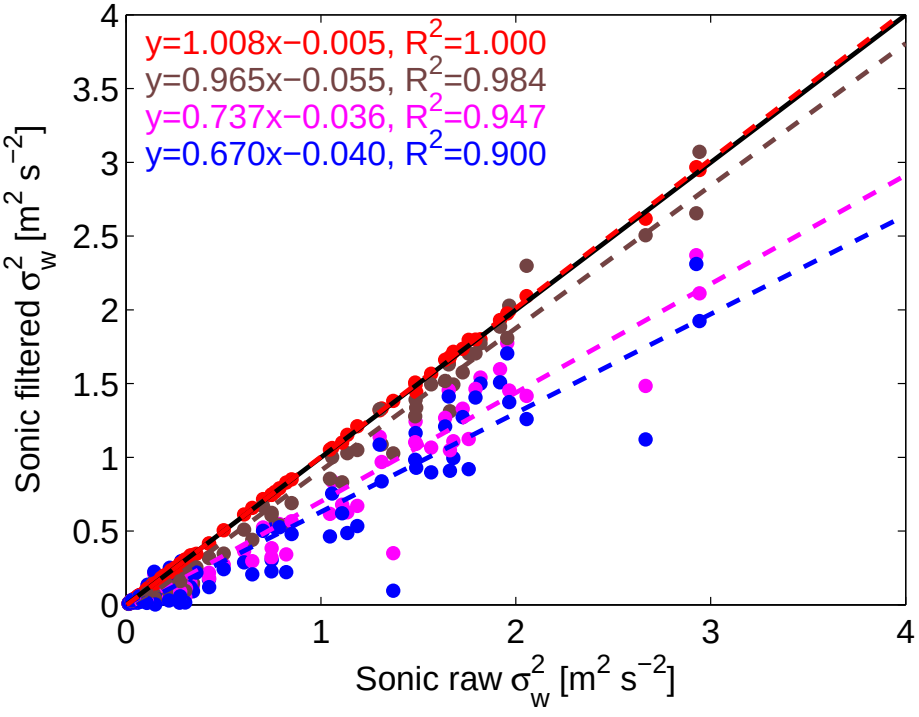

Figure 6. Relation of σ_w^2 values computed from the raw 30-min sonic timeseries compared with those estimated from the fitting of Eq. 4 to the filtered sonic anemometer data at 300-m. Red and brown dots are the estimate from sonic data averaged to 1-Hz and 0.1-Hz respectively, after the fitting is applied using the specified number of lags discussed in Sect. 3.2. Magenta and blue dots are estimates from sonic data averaged to 1-Hz and 0.1-Hz, after the fitting is applied using 100 s of lag time. Black line indicates a one-to-one relationship. The dashed lines show the linear regressions, with the equations for linear regression and coefficients of determination shown in the upper left corner.

However, since the linear regression line for the 0.1 Hz data (red line in Fig. 6) follows nearly a one-to-one relationship and coefficient of determination is ≈ 1, the fitting is good for all lag times used and the random error due to the variable lag time is small.

However, when 100 s of lag time is used within the fitting of the structure function, estimates of σ_w^2 are generally grossly underestimated regardless of the averaging time. This lag time should never be applied under stable conditions since the inertial subrange is small. Additionally, 100 s lag time is too large during unstable conditions as well, leading to underestimates of σ_w^2. Furthermore, since σ_w^2 is underestimated, values of t_{int} as defined in Eq. 9 will be overestimated, leading to the inaccurate interpretation that a larger number of lags is acceptable to use.

Atmos. Meas. Tech. Discuss., doi:10.5194/amt-2016-134, 2016
Manuscript under review for journal Atmos. Meas. Tech.
Published: 7 July 2016

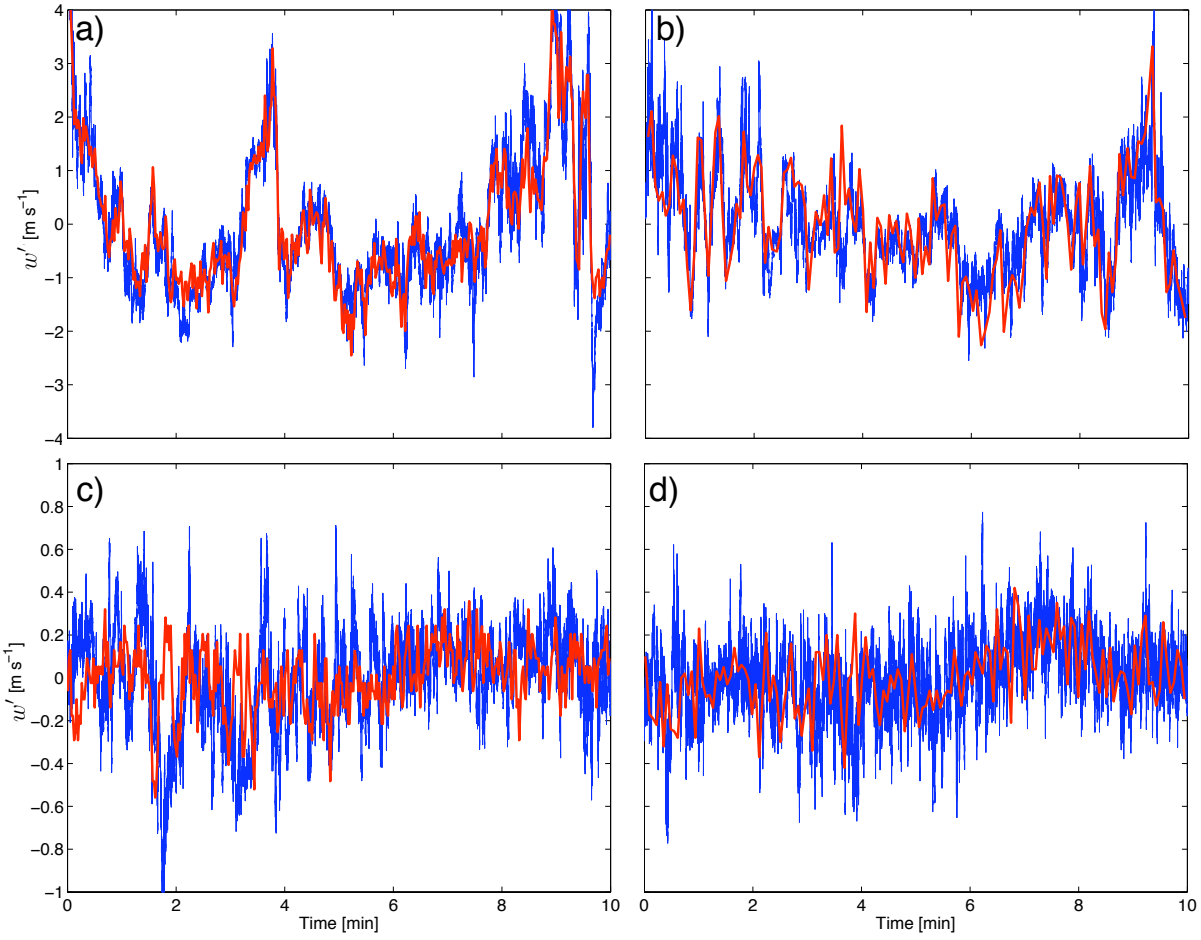

Figure 7. Timeseries of w' during unstable (a, b) and stable (c, d) conditions, with each stability being during the same 10-min time periods when the sonic anemometer is not waked by the 300-m tower. OU DL data are at 300-m (a, c), and LLNL WC measurements are at 100-m (b, d). Red line shows the DL timeseries, while the blue line shows the comparable timeseries from the collocated sonic at the same height. Note that y-axis scales for w' are different in the top and bottom panels.

4.2 Comparison of Timeseries of w from DLs and Sonic Anemometers

Example timeseries of w' from each DL compared with similar measurements from sonic anemometers are shown in Fig. 7 for both convective and stable periods. Generally, measurements from both the sonics and DLs tend to show similar trends in how w' varies over time. Maxima and minima of w' occur at nearly the same time, which is particularly apparent in Fig. 7a, b where the fluctuations are much larger. The magnitude of each individual maximum/minimum of w' is generally less in the DL observations as compared to those from the sonic anemometers. The longer time and larger volume averaging of the DLs reduces the magnitude of its observed fluctuations. Additionally, both DLs do not resolve all of the fluctuations that occur at

Atmos. Meas. Tech. Discuss., doi:10.5194/amt-2016-134, 2016
Manuscript under review for journal Atmos. Meas. Tech.
Published: 7 July 2016

Atmospheric Measurement Techniques Discussions

short timescales. Differences in sampling frequency of the OU DL and LLNL WC are evident, particularly in Fig. 7a, b. Since the LLNL WC has a lower sampling rate than the OU DL, turbulence statistics computed from its measurements are not as representative of the true atmospheric variance as those from the OU DL.

Observations during stable conditions, shown in Fig. 7c, d, show less agreement in the time evolution of w' between the DL and sonic anemometer measurements compared to those during unstable conditions. This can be explained by the fact that during more neutral/unstable conditions atmospheric turbulence is governed by large turbulent eddies while during stable conditions much smaller eddies, which cannot be fully resolved by DL measurements, dominate. Differences in sampling volume and frequency thus have stronger effects during stable conditions, explaining why the scatter between the two different DLs becomes larger during stable than unstable conditions.

4.3 Comparison of DL and Sonic Spectra and Autocovariance Function

Several examples of M_{11} and the spectra of w from the OU DL and LLNL WC, compared with similar statistics from the collocated sonic anemometer, are shown in Figs. 8, 9. The cases were chosen to show the accuracy of the DL spectra and M_{11} under various conditions. Measurements from the sonic anemometer are averaged to replicate the averaging time and sampling frequency for each DL, to isolate how these parameters affect the measurement and evaluate the accuracy of using the method discussed in Sect. 3. Generally, the spectra for the OU DL show good agreement with those calculated from sonic anemometer measurements. Under all of the cases presented, the lower frequency end of the inertial subrange is captured by the OU DL, as a portion of the spectra follows the theoretical -2/3 line. However, at high frequencies ($f > 0.1$ Hz) within Fig. 8b, d, the OU DL spectra flattens out or increases, which is likely due to a combination of noise in the signal increasing the variance and spectral aliasing. Noise within the OU DL spectra in Fig. 8f is large enough to cause an increase in the spectra at high frequencies. Additionally, within both the OU DL and downsampled sonic spectra shown in Fig. 8, the flattening of the spectra at the highest resolved frequencies is due to spectral aliasing from the smallest-scale turbulent motions being undersampled in time (see Kirchner, 2005).

While the spectra of w' from the OU DL are generally in agreement with those from the sonic anemometers, significant differences are apparent in M_{11} computed from the two instruments (Fig. 8a, c, e). For example, within Fig. 8a, M_{11} values are similar for short lags up to 10 s, after which M_{11} computed from the OU DL is greater than that from the sonic anemometer. On the contrary, within the time period for Fig. 8e, the values of M_{11} are in better agreement at larger lags (greater than 30 s), but the OU DL derived M_{11} is much less than those computed from the sonic anemometers at shorter lags. The reasons for these differences are not clear, but are likely due to differing measurement volumes. The anemometer samples a volume of air precisely at 300 m, while the comparable OU DL measurement is averaged over a layer between 288–306 m. Thus, the exact measurements of w, and its derived statistics, are expected to be slightly different between the sonic anemometer and DL.

Within all three cases shown in Fig. 8, $M_{11}(0)$ calculated from the OU DL measurements is smaller than that calculated from the sonic anemometer measurements. This indicates that, within these cases, the variance is underestimated by the OU DL. Using the structure function fit, the estimated values of the variance from the OU DL data are improved for the cases shown in Fig. 8a, c. Within Fig. 8e, the fitting leads to a smaller value of OU DL-derived σ_w^2, due to the fact that noise is present as

Atmos. Meas. Tech. Discuss., doi:10.5194/amt-2016-134, 2016
Manuscript under review for journal Atmos. Meas. Tech.
Published: 7 July 2016

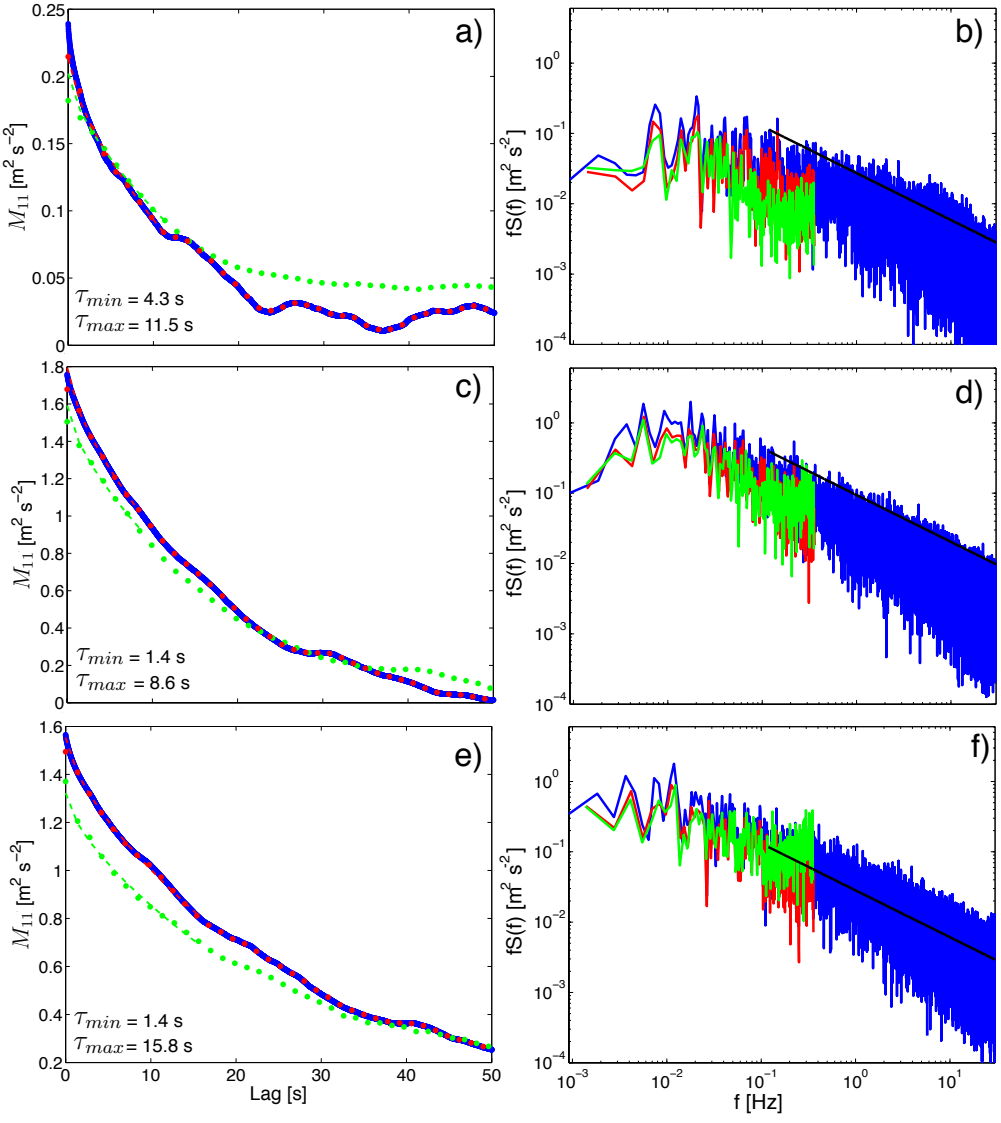

Figure 8. Sample M_{11} (left column) and the corresponding spectra (right column) averaged over different 30-min time periods for measurements at 300-m. Measurements shown are those calculated from the raw sonic observations (blue), sonic data averaged to match the lidar averaging time (red), and OU DL observations (green). Dashed lines overlaid on M_{11} are the fittings of the structure function fit to the corresponding measurement. The fitting for the filtered sonic data use the same lags as that for the DL. M_{11} and the spectra are computed over 0530–0600 UTC (a, b), 1730–1800 UTC (c, d), and 2300–2330 UTC (e, f) on 27 March. Observations in a, b are during stable conditions (Ri$= 0.64$), while data shown in c, d, e, f are during near neutral conditions($|Ri| < 0.05$). Values of τ_{max} and τ_{min} for each time period are shown in the lower left of (a, c, e).

Atmos. Meas. Tech. Discuss., doi:10.5194/amt-2016-134, 2016
Manuscript under review for journal Atmos. Meas. Tech.
Published: 7 July 2016

Atmospheric Measurement Techniques Discussions

shown in Fig. 8f. By applying the structure function fit to the sonic anemometer measurements that are averaged to simulate the OU DL observations, it is shown that the fitting uses a proper number of lags to estimate the expected M_{11} to lag zero. The effect of averaging time on retrieved estimates of variance is discussed more throughly in Sect. 4.1.

Based on the presented spectra in Fig. 9b, d, f, LLNL WC w' spectra are in generally good agreement at most frequencies with those derived from sonic anemometer measurements. Similarly to the OU DL spectra, the LLNL WC spectra are often larger than those from the anemometers at high frequencies due to noise in the signal and spectral aliasing of higher frequencies that are not resolved by the reduced sampling rate. The LLNL WC is often, but not always, able to resolve the lower frequency portion of the inertial subrange. Within the convective conditions shown in Fig. 9d, f, the high-frequency region of the LLNL WC spectra follows the -2/3-law expected within the inertial subrange. However, within the time period shown in Fig. 9b, the inertial subrange is not resolved due to the fact that turbulence scales are small and that the sampling frequency of 0.25 Hz is not fast enough to capture the smaller turbulence scales.

Generally, the values of M_{11} at various lags computed from either the LLNL WC or sonic anemometers are in agreement with each other. However, differences in M_{11} do exist due to similar reasons to those discussed for the OU DL. For time periods when the lower frequency portion of the inertial subrange could be resolved (i.e., in Fig. 9c, e), the structure function fitting yields an improved estimate for σ_w^2 compared to the raw variance at $M_{11}(0)$, that is closer to the sonic-derived value. However, when no portion of the inertial subrange is resolved, the fitting of Eq. 4 poorly models the true values of M_{11} at short lags and the estimated value of σ_w^2 is grossly underestimated. This is expected, as the fitted function only applies within the inertial subrange.

4.4 Accuracy of DL Variance Estimates

Comparisons of 30-min averaged σ_w^2 from the DL observations, which were either directly computed or estimated using the structure function fitting, compared with those from sonic anemometers are shown in Fig. 10. For both the LLNL WC and OU DL, using the structure function fitting to estimate values of σ_w^2 generally provided more accurate and less biased values, based on the higher values of R^2, a slope of the best-fit line closer to one, and y-intercept closer to zero compared to the values computed directly from the timeseries. The greater scatter in the LLNL WC measurement is attributed to its reduced sampling frequency. Since there are 3 s gaps in its measurements of w while it collects data at off-zenith angles for the DBS scan, values of σ_w^2 computed from the LLNL WC are not as robust as those from the OU DL, which took w measurements continuously with a sampling frequency of 0.7 Hz. Still, LLNL WC estimates of σ_w^2 are in generally good agreement ($R^2 \approx 0.9$) with those from the sonic anemometers and show low bias when using the autocovariance fitting.

For the OU DL, estimates of σ_w^2 are generally improved when using the structure function fitting for the entire range of variance values. When the raw OU DL σ_w^2 value is lower than the sonic value, the autocovariance technique generally increases the estimate of σ_w^2. Conversely, when significant noise is present and the raw OU DL σ_w^2 is greater than the sonic value, the autocovariance technique generally reduces the estimate of σ_w^2 improving the estimate. This is particularly evident in Fig. 10b, where there are a cluster of points of uncorrected σ_w^2 that are much larger than the true atmospheric variance. These overestimates are coincident with a time period when the OU DL SNR was reduced. For estimates of σ_w^2 from the LLNL WC,

Atmos. Meas. Tech. Discuss., doi:10.5194/amt-2016-134, 2016
Manuscript under review for journal Atmos. Meas. Tech.
Published: 7 July 2016

Atmospheric Measurement Techniques Discussions

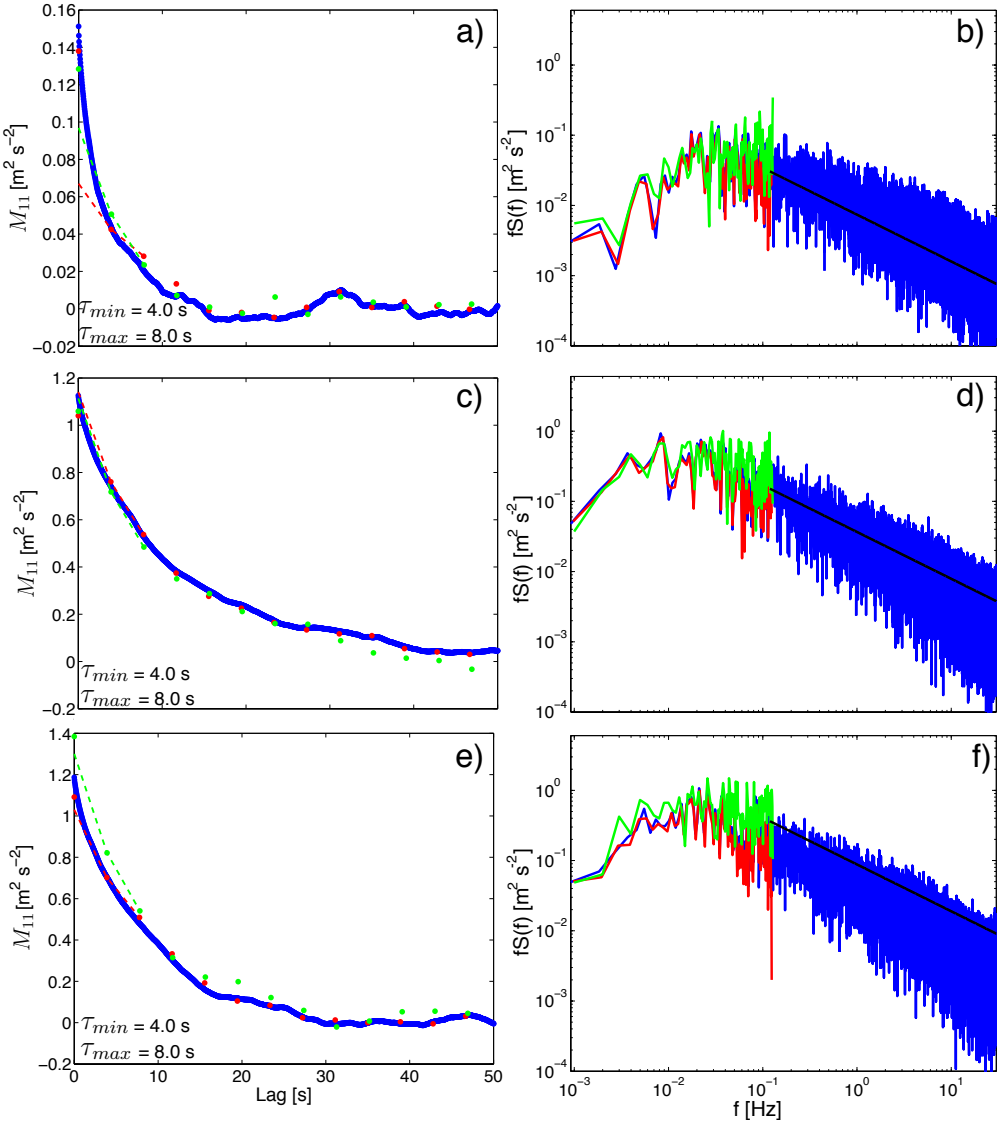

Figure 9. Sample M_{11} (left column) and the corresponding spectra (right column) averaged over different 30-min time periods for measurements at 100-m. The spectra are made by averaging 10-min spectra within the 30-min time period to reduce the noise within the spectra. Measurements shown are those calculated from the raw sonic observations (blue), sonic data averaged to match the lidar averaging time (red), and LLNL WC observations (green). Dashed lines overlaid on M_{11} are the fittings of the structure function fit to the corresponding measurement. The fitting for the filtered sonic data use the same lags as that for the DL. M_{11} and the spectra are computed over 0030–0100 UTC (a, b), 2130–2200 UTC (c, d), and 1730–1800 UTC (e, f) on 27 March. Values of τ_{max} and τ_{min} for each time period is shown in the lower left of (a, c, e).

Atmos. Meas. Tech. Discuss., doi:10.5194/amt-2016-134, 2016
Manuscript under review for journal Atmos. Meas. Tech.
Published: 7 July 2016

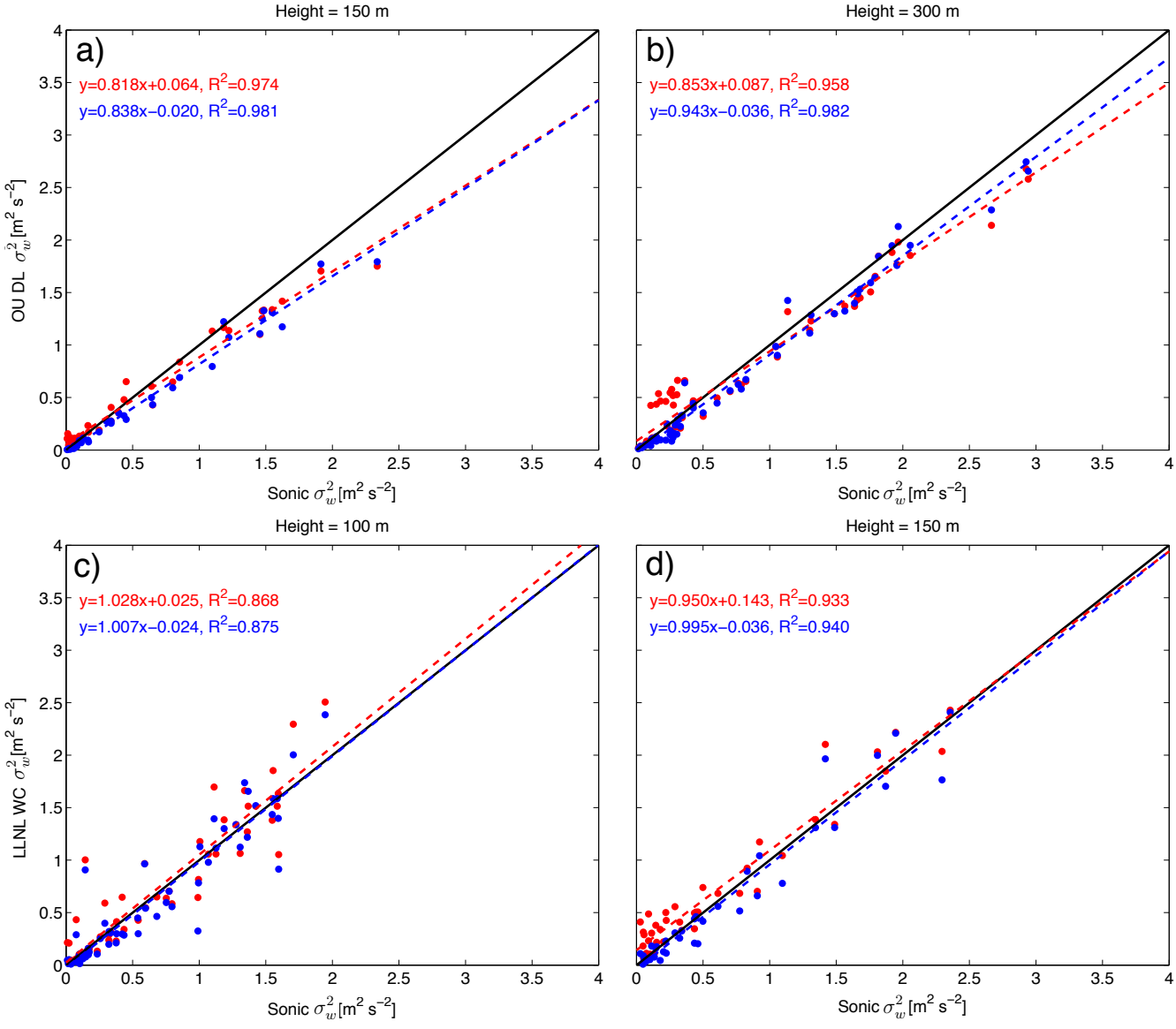

Figure 10. Comparison of σ_w^2 computed from DL observations with those from the sonic anemometer observations at different heights. Heights were chosen to highlight differences in the quality of observations with height, and where high-quality sonic and lidar observations are available. Observations from the OU DL are shown in (a, b), while LLNL WC measurements are shown in (c, d). Red denotes σ_w^2 computed from the raw DL data (i.e., $M_{11}(0)$), while blue is for values wherein σ_w^2 is taken as $M_{11}^*(0)$. Equations of the best fits are shown in the upper left of each plot, with R^2 being the coefficient of determination. Values of σ_w^2 are averaged over 30-min windows.

directly-computed values of σ_w^2 are generally larger than those computed from the structure function fitting regardless of the magnitude of the turbulence. Again, the autocovariance fitting accurately removes the contribution of noise in the measured

Atmos. Meas. Tech. Discuss., doi:10.5194/amt-2016-134, 2016
Manuscript under review for journal Atmos. Meas. Tech.
Published: 7 July 2016

Atmospheric Measurement Techniques Discussions

σ_w^2, which is particularly apparent when σ_w^2 is less than 0.5 m^2 s^{-2} in Fig. 10d. For time periods when turbulence is strong, the autocovariance fitting to the LLNL WC data often leads to reduced values of σ_w^2; this could be due to increased noise in the LLNL WC observations compared to those from the OU DL under similarly strongly turbulent conditions, or the fact that the structure function fitting is not as accurate with a smaller number of lags used due to the reduced sampling rate of the LLNL WC compared to the OU DL.

4.5 Effect of Turbulence Characteristics and Stability

As shown earlier, the DL must be able to resolve a portion of the inertial subrange in order to accurately extract measurements of σ_w^2. If part of the inertial subrange is not explicitly resolved when turbulence scales are small, then a proper fitting that is representative of how M_{11} actually varies at small lags cannot be accurately applied. Regardless, even in these conditions when turbulence is weak, it is especially important to not simply use σ_w^2 directly computed from the timeseries, as ϵ^2 is often a large component of the computed σ_w^2, as shown for small values of σ_w^2 in Fig. 10b, d. Thus, even for these cases, applying the structure function fitting generally provides more accurate estimates of σ_w^2, although $M_{11}^*(0)$ values are systematically underestimates of the true variance.

For the OU DL, estimates of σ_w^2 are generally in better agreement at 300 m than at lower heights. In fact, during the two-day observational period, σ_w^2 generally is more underestimated at lower heights reflected in the slope of the best fit line decreasing. While the reason for this is not entirely clear, it is thought that the more accurate measurements are made at higher heights due to the fact that eddies are larger further from the ground, which are better resolved by the DL. These differences in how the accuracy of lidar variance measurements change with height needs to be considered when evaluating how second- and higher-order statistics vary with height.

The relationship between the accuracy of turbulence parameters measured by both DLs and stability, specifically Ri, during those observations is shown in Fig. 11. During netural/unstable conditions when Ri is close to zero or negative, the estimates of σ_w^2 from both DLs are generally more accurate than those measurements during stable conditions. This is evident based on the lower scatter and ratios of σ_w^2 closer to one under unstable conditions for both uncorrected and corrected estimates. Additionally, especially for OU DL measurements, the corrected measurements during convective conditions are larger and more accurate than those that are uncorrected. When conditions are stable, there is substantially more scatter in the quality of the DL measurements and the improvement due to the structure function fitting is less clear. There are times when the correction technique improves the σ_w^2 estimates, such as when significant noise is present that is accurately removed. These time periods also tend to occur when SNR is reduced, as shown in Fig. 12. The method also can lead to worse estimates of σ_w^2, when turbulence scales are small and the inertial subrange is not properly resolved by the DLs. However, applying the extrapolation technique during stable conditions generally improves the estimates of σ_w^2. Although values of σ_w^2 are systematically underestimated when determined from the extrapolation method during stable conditions, the values are more comparable with each other than uncorrected measurements.

Atmos. Meas. Tech. Discuss., doi:10.5194/amt-2016-134, 2016
Manuscript under review for journal Atmos. Meas. Tech.
Published: 7 July 2016

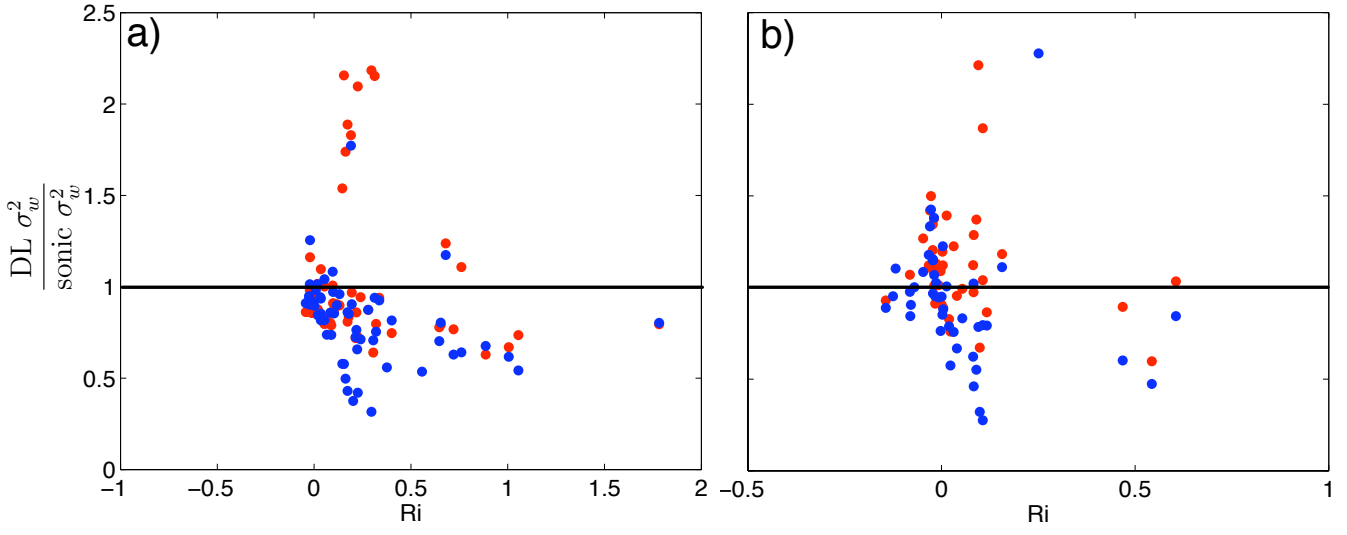

Figure 11. Relation of stability with error in lidar measured σ_w^2, as compared to σ_w^2 computed from sonic anemometer measurements, for raw (red) and corrected (blue) measurements. Measurements from the OU DL at 300-m are shown in a), while LLNL WC measurements at 100-m are shown in b). For some time periods under stable conditions (e.g., Ri greater than 0.25), uncorrected DL measurements have very high error, the ratio is greater than 2, and points are off the graph. During the study period, the conditions were predominantly near-neutral, which is why there are fewer data points during stable conditions.

5 Discussion

Below, recommendations are made as to the implementation of this technique for use with DLs based on these results. Additionally, the importance of validation studies for measurements from various types of lidars is discussed.

5.1 Possible Applications to Other DL Scanning Techniques

Within Sect. 4, it is shown that the autocovariance technique can be used to improve DL turbulence measurements, specifically σ_w^2 here, by both removing noise and correcting for unresolved turbulence structures. This method could similarly be applied to measurements of other turbulent quantities. For instance, for a DL continuously pointing at a very low elevation (near zero) into the wind, values of σ_u^2 can be derived by using a similar technique. Furthermore, this technique could be applied to be used in conjunction with more advanced scanning strategies. For turbulence measurements using the six-beam scanning strategy (Sathe et al., 2015), variances are first computed for each of the six independent beams. The six components of the Reynolds stress tensor can be computed from the individual variances of the six beams. However, due to the equations of computing each component of the Reynolds stress tensor, the effect of noise within each individual measurement is magnified. In particular, if there is a large amount of noise in the vertical beam compared to other beams from differences in SNR, then negative values of σ_u^2 and σ_v^2 can be computed (Newman et al., 2015), which is not realistic. Thus, if the observations within each beam are taken

Atmos. Meas. Tech. Discuss., doi:10.5194/amt-2016-134, 2016
Manuscript under review for journal Atmos. Meas. Tech.
Published: 7 July 2016

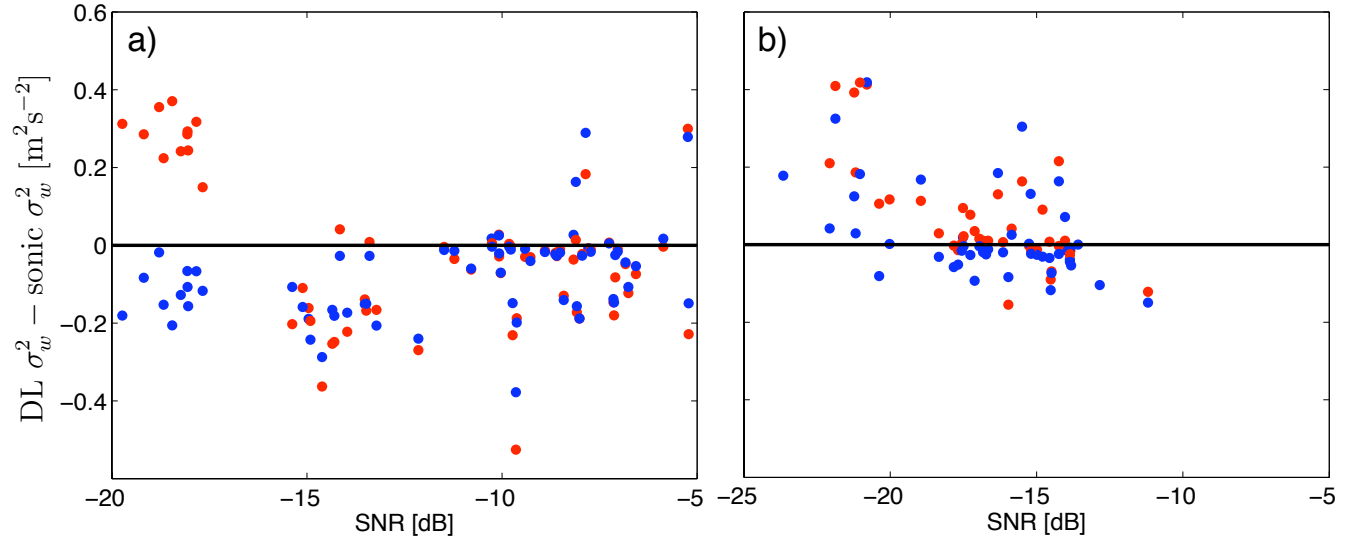

Figure 12. Relation of SNR with error of lidar measured σ_w^2, as compared to σ_w^2 computed from sonic anemometer measurements, for raw (red) and corrected (blue) measurements. Measurements from the OU DL at 300-m are shown in a), while LLNL WC measurements at 100-m are shown in b).

at a large enough sampling rate to resolve the inertial subrange, the autocovariance technique should be applied to variances calculated from each beam before computing the velocity variances.

5.2 Importance of Validation Studies for Various Types of Lidars

Remote sensors, such as lidars, provide the ability to measure various quantities throughout the atmosphere. However, it is imperative that these measurements are compared with in situ observations for validation. Through this, relative accuracies can be quantified, so that future measurements using only remote sensors can be correctly interpreted and utilized. While the first in-depth analysis of σ_w^2 estimates measured using a method proposed by Lenschow et al. (2000) are presented here, further intercomparison studies of DL and in situ measurements are needed. Since this study was conducted over a short two-day period in early spring, the atmospheric conditions were not representative of the wide range that may occur over the entire year. Additionally, the measurement comparisons all were within the lowest 300-m of the PBL. While this provided a larger overlap region than allowed by most conventional meteorological towers, it still only encompasses a fraction of the possible PBL depth. As discussed in Sect. 4.4, there is evidence that biases in DL σ_w^2 change with height, which needs to be investigated further. These biases will affect how the DL-measured profiles of σ_w^2 vary with height.

In addition, measurements of higher-order moments from other types of lidars, such as DIALs and Raman lidars, should also be compared with in situ measurements. Due to the larger averaging time and often larger lag times used, errors associated with these lidars are likely higher and measured quantities are likely biased low, as discussed in Sect. 4.1. Turner et al. (2014a) compared Raman lidar-derived estimates of water vapour variance and skewness with those measured from aircraft, showing

Atmos. Meas. Tech. Discuss., doi:10.5194/amt-2016-134, 2016
Manuscript under review for journal Atmos. Meas. Tech.
Published: 7 July 2016

Atmospheric Measurement Techniques Discussions

general good agreement in the trends in the profiles. However, the accuracy of the values of the DIAL and Raman lidar higher-order moments should be carefully evaluated.

6 Summary and Conclusions

Here, a method discussed by Lenschow et al. (2000) of measuring higher-order statistics using autocovariances from lidar data is carefully evaluated. Specifically, estimates of vertical velocity variance and integral timescales derived from DL observations are compared with similar measurements from collocated sonic anemometers. Two DLs, a WindCube v2 and a Halo Streamline, were placed within a few metres of the 300-m tower at the Boulder Atmospheric Observatory in Erie, Colorado, USA from 26 to 28 March 2014. The tower was instrumented with sonic anemometers at 50 m intervals, up to 300 m, for validation and comparison of measurements from the DL.

The impact of several parameters on the accuracy and quality of lidar variance estimates is investigated using two methods. First, sonic anemometer observations are averaged to simulate typical averaging times of different types of lidars, after which the autocovariance technique is used with various lag times to retrieve the variance values. Secondly, variances computed from the sonic anemometers are compared with those from the DL observations, both of those computed directly and using the autocovariance technique. Through these comparisons, it is shown that

- The amount of lag time used within the fitting of the structure function to the autocovariance is critical for accurate estimates of σ_w^2, and the number of lags leading to accurate retrievals of variance estimates are defined herein. Long lag times, which are generally used when extracting higher-order moments from DIALs and Raman lidars, lead to gross underestimates of the true atmospheric variance.

- Not only does the autocovariance method accurately remove contributions from noise, but it also can be used to correct for limitations of time and volume averaging in the measurements. Thus, short lag times, for which the small-scale turbulent eddies are not accurately sampled (i.e., less than τ_{min}), should not be used when applying the fitting of the structure function.

- Generally, estimates of the vertical velocity variance from the DLs agree with those computed from sonic anemometers at the same measurement height, especially during unstable conditions. Small differences in the measurements can be attributed to differences in averaging volumes (and averaging heights). For the WindCube v2, more substantial differences in the measurements are due to the reduced sampling rate of the measurements, as vertical velocity is only measured every 4 s. By applying the autocovariance method, estimates of DL vertical velocity variance measurements are generally improved, even when turbulence is weak under stable conditions since small amounts of noise are a larger proportion of the total measured variance.

The importance of intercomparison studies for remote sensor measurements is highlighted. In particular, techniques for retrieving various derived-statistics can be validated and refined through the intercomparison of remote sensor measurements

Atmos. Meas. Tech. Discuss., doi:10.5194/amt-2016-134, 2016
Manuscript under review for journal Atmos. Meas. Tech.
Published: 7 July 2016

with high-quality in situ observations. Limitations in the applicability of the techniques can be identified as well. Since it is shown that DL-derived turbulence measurements are generally improved by applying the autocovariance techniques, it is believed that this method can be applied to more measurements taken using more advanced scanning strategies, such as the six-beam technique.

Acknowledgements. We acknowledge NOAA ESRL and NCAR for all the support in deploying the instruments during LATTE and for allowing this experiment to be conducted at the BAO site. We thank Andreas Muschinski, Lucas Root, and Shiril Tichkule for their assistance in installing and maintaining the sonic anemometers on the tower. Input and comments from David Turner and Alan Shapiro were very helpful. This work was supported by funding from the Office of the Vice President for Research at the University of Oklahoma, the National Center for Atmospheric Research (NCAR) Faculty Fellowship Program, and NCAR Earth Observing Laboratory.

Atmos. Meas. Tech. Discuss., doi:10.5194/amt-2016-134, 2016
Manuscript under review for journal Atmos. Meas. Tech.
Published: 7 July 2016

Atmospheric Measurement Techniques Discussions

References

Alvarez II, R. J., Senff, C. J., Langford, A. O., Weickmann, A. M., Law, D. C., Machol, J. L., Merritt, D. A., Marchbanks, R. D., Sandberg, S. P., Brewer, W. A., Hardesty, R. M., and Banta, R. M.: Development and application of a compact, tunable, solid-state airborne Ozone lidar system for boundary layer profiling, J. Atmos. Ocean. Tech., 28, 1258–1272, 2011.

Banta, R. M., Pichugina, Y. L., and Brewer, W. A.: Turbulent velocity-variance profiles in the stable boundary layer generated by a nocturnal low-level jet, J. Atmos. Sci., 63, 2700–2719, 2006.

Barlow, J. F., Dunbar, T. M., Nemitz, E. G., Wood, C. R., Gallagher, M. W., Davies, F., O'Connor, E., and Harrison, R. M.: Boundary layer dynamics over London, UK, as observed using Doppler lidar during REPARTEE-II, Atmos. Chem. Phys., 11, 2111–2125, 2011.

Behrendt, A., Wulfmeyer, V., Hammann, E., Muppa, S. K., and Pal, S.: Profiles of second- to third-order moments of turbulent temperature fluctuations in the convective boundary layer: first measurements with Rotational Raman Lidar, Atmos. Chem. Phys., 15, 5485–5500, 2015.

Brinkmann, W. A. R.: Strong downslope winds at Boulder, Colorado, Mon. Wea. Rev., 102, 592–602, 1974.

Davies, F., Collier, C. G., Pearson, G. N., and Bozier, K. E.: Doppler lidar measurements of turbulent structure function over an urban area, J. Atmos. Ocean. Tech., 21, 753–761, 2004.

Davis, J. C., Collier, C. G., Davies, F., and Bozier, K. E.: Spatial variations of sensible heat flux over and urban area measured using Doppler lidar, Meteorol. Appl., 15, 367–380, 2008.

Dunbar, T. M., Barlow, J. F., and Belcher, S. E.: An optimal inverse method using Doppler lidar measurements to estimate the surface sensible heat flux, Boundary-Layer Meteorol., 150, 49–67, 2014.

Eberhard, W. L., Cupp, R. E., and Healy, K. R.: No Title, J. Atmos. Ocean. Tech., 6, 809–819, 1989.

Frehlich, R. and Cornman, L.: Estimating spatial velocity statistics with coherent Doppler lidar, J. Atmos. Ocean. Techn., 19, 355–366, 2002.

Frehlich, R. G. and Yadlowsky, M. J.: No Title, J. Atmos. Ocean. Tech., 11, 1217–1230, 1994.

Fuertes, F. C., Iungo, G. V., and Porté-Agel, F.: 3D Turbulence measurements using three synchronous wind lidars: Validation against sonic anemometry, J. Atmos. Ocean. Tech., 31, 1549–1556, 2014.

Gal-Chen, T., Xu, M., and Eberhard, W. L.: Estimations of Atmospheric Boundary Layer Fluxes and other Turbulence parameters from Doppler Lidar data, J. Geophys. Res., 97, 18 409–18 423, 1992.

Grund, C. J., Banta, R. M., George, J. L., Howell, J. N., Post, M. J., Richter, R. A., and Weickmann, A. M.: High-resolution Doppler lidar for boundary layer and cloud research, J. Atmos. Ocean. Tech., 18, 376–393, 2001.

Higgins, C. W., Froidevaux, M., Simeonov, V., Vercauteren, N., Barry, C., and Parlange, M. B.: The effect of scale on the applicability of Taylor's frozen turbulent hypothesis in the atmospheric boundray layer, Boundary-Layer Meteorol., 143, 379–391, 2013.

Hogan, R. J., Grant, A. L. M., Illingworth, A. J., Pearson, G. N., and O'Connor, E. J.: Vertical velocity variance and skewness in clear and cloud-topped boundary layers as revealed by Doppler lidar, Q. J. R. Meteorol. Soc., 135, 635–643, 2009.

Hollinger, D. Y. and Richardson, A. D.: Uncertainty in eddy covariance measurements and its application to physiological models, Tree Physiol, 25, 873–885, 2005.

Kaimal, J. C. and Gaynor, J. E.: The Boulder Atmospheric Observatory, J. Clim. Appl. Meteorol., 22, 863–880, 1983.

Kirchner, J. W.: No Title, Phys. Rev. E, 71, 66 110, 2005.

Kolmogorov, A.: The local structure of turbulence in incompressible viscous fluid for very large Reynolds' numbers, Dokl. Akad. Nauk. SSSR, 30, 301–305, 1941.

Krishnamurthy, R., Calhoun, R., Billings, B., and Doyle, J.: Wind turbulence estimates in a valley by coherent Doppler lidar, Meteorol. Appl., 18, 361–371, 2011.

Lenschow, D. H., Mann, J., and Kristensen, L.: How long is long enough when measuring fluxes and other turbulence statistics?, J. Atmos. Ocean. Tech. Technol., 11, 661–673, 1994.

Lenschow, D. H., Wulfmeyer, V., and Senff, C.: Measuring Second- through fourth-order moments in noisy data, J. Atmos. Ocean. Tech., 17, 1330–1347, 2000.

Lenschow, D. H., Lothon, M., Major, S. D., Sullivan, P. P., and Canut, G.: A comparison of higher-order vertical velocity moments in the convective boudnary layer from lidar with in situ measurements and large-eddy simulation, Boundary-Layer Meteorol., 143, 107–123, 2012.

Lindseth, B., Brown, W. O. J., Jordan, J., Law, D., Hock, T., Cohn, S. A., and Popović, Z.: A new portable 449-MHz spaced antenna wind profiler radar, IEEE Trans. Geosci. Remote Sens., 50, 3544–3553, 2012.

Lothon, M., Lenschow, D. H., and Major, S. D.: Coherence and scale of vertical velocity in the convective boundary layer from a Doppler lidar, Boundary-Layer Meteorol., 121, 521–536, 2006.

Lothon, M., Lenschow, D. H., and Major, S. D.: Doppler lidar measurements of vertical velocity spectra in the convective boundary layer, Boundary-Layer Meteorol., 132, 205–226, 2009.

Machol, J. L., Ayers, T., Schwenz, K. T., Koenig, K. W., Hardesty, R. M., Senff, C. J., Krainak, M. A., Abshire, J. B., Bravo, H. E., and Sandberg, S. P.: Preliminary measurements with an automated compact differential absorption lidar for profiling of water vapor, Appl Opt., 43, 3110–3121, 2004.

Machol, J. L., Marchbanks, R. D., Senff, C. J., McCarty, B. J., Eberhard, W. L., Brewer, W. A., Richter, R. A., II, R. J. A., Law, D. C., Weickmann, A. M., and Sandberg, S. P.: Scanning tropospheric ozone and aerosol lidar with double-gated photomultipliers, Appl Opt., 48, 512–524, 2009.

Mahrt, L.: Flux Sampling Errors for Aircraft and Towers, J. Atmos. Ocean. Technol., 15, 416–429, 1998.

Mauder, M., Cuntz, M., Drüe, C., Graf, A., Rebmann, C., Schmid, H. P., Schmidt, M., and Steinbrecher, R.: A strategy for quality and uncertainty assessment of long-term eddy-covariance measurements, Agr. For. Meteorol., 169, 122–135, 2013.

McNicholas, C. and Turner, D. D.: Characterizing the convective boundary layer turbulence with a High Spectral Resolution Lidar, J. Geophys. Res.-Atmos., 119, 12 910–12 927, 2014.

Monin, A. S. and Yaglom, A. M.: Statistical Fluid Mechanics, MIT Press, pp. 874, 1979.

Newman, J. F., Klein, P. M., Wharton, S., Sathe, A., Bonin, T. A., Chilson, P. B., and Muschinski, A.: Evaluation of three lidar scanning strategies for turbulence measurements, Atmos. Meas. Tech. Discuss., 8, 12 329–12 381, 2015.

O'Connor, E. J., Illingworth, A. J., Brooks, I. M., Westbrook, C. D., Hogan, R. J., Davies, F., and Brooks, B. J.: A method for estimating the turbulence kinetic energy dissipation rate from a vertically pointing Doppler lidar, and independent evaluation from balloon-borne in situ measurements, J. Atmos. Ocean. Tech., 27, 1652–1664, 2010.

Pearson, G., Davies, F., and Collier, C.: An analysis of the performance of the UFAM pulsed Doppler lidar for observing the boundary layer, J. Atmos. Ocean. Tech., 26, 240–250, 2009.

Pearson, G., Davies, F., and Collier, C.: Remote sensing of the tropical rain forest boundary layer using pulsed Doppler lidar, Atmos. Chem. Phys., 10, 5891–5901, 2010.

Peltola, O., Hensen, A., Helfter, C., Belelli Marchesini, L., Bosveld, F. C., van den Bulk, W. C. M., Elbers, J. A., Haapanala, S., Holst, J., Laurila, T., Lindroth, A., Nemitz, E., R/"ockmann, T., Vermeulen, A. T., and Mammarella, I.: Evaluating the performance of commonly

used gas analysers for methane eddy covariance flux measurements: the InGOS inter-comparison field experiment, Biogeosciences, 11, 3163–3186, 2014.

Pichugina, Y. L., Banta, R. M., Kelley, N. D., Jonkman, B. J., Tucker, S. C., Newsom, R. K., and Brewer, W. A.: Horizontal-velocity and variance measurements in the stable boundary layer using Doppler lidar: Sensitivity to averaging procedures, J. Atmos. Ocean. Tech., 25, 1307–1327, 2008.

Sathe, A. and Mann, J.: A review of turbulence measurements using ground-based wind lidars, Atmos. Meas. Tech., 6, 3147–3167, 2013.

Sathe, A., Mann, J., Vasiljevic, N., and Lea, G.: A six-beam method to measure turbulence statistics using ground-based wind lidars, Atmos. Meas. Tech., 8, 729–740, 2015.

Shukla, K. K., Phanikumar, D. V., Newsom, R. K., Kumar, K. N., Ratman, M. V., Naja, M., and Singh, N.: Estimation of the mixing layer height over a high altitude site in Central Himalayan region by using Doppler lidar, J. Atmos. Sol.-Terr. Phy., 48-53, 48–53, 2014.

Smith, D. A., Harris, M., Coffey, A. S., Mikkelsen, T., Jørgensen, H. E., Mann, J., and Danielian, R.: Wind Lidar evluation at the Danish wind test site in Høvsøre, Wind Energy, 9, 87–93, 2006.

Taylor, G. I.: The spectrum of turbulence, Proc. Roy. Soc., A164, 476–490, 1938.

Tucker, S. C., Brewer, W. A., Banta, R. M., Senff, C. J., Sandberg, S. P., Law, D. C., Weickmann, A. M., and Hardesty, R. M.: Doppler lidar estimation of mixing height using turbulence, shear, and aerosol profiles, J. Atmos. Ocean. Tech., 26, 673–688, 2009.

Turner, D. D., Ferrare, R. A., Wulfmeyer, V., and Scarino, A. J.: Aircraft evaluation of ground-based Raman lidar water vapor turbulence profiles in convective mixed layers, J. Atmos. Ocean. Tech., 31, 1078–1088, 2014a.

Turner, D. D., Wulfmeyer, V., Berg, L. K., and Schween, J. H.: Water vapor turbulence profiles in stationary continental convective mixed layers, J. Geophys. Res.-Atmos., 119, 11 151–11 165, 2014b.

Wulfmeyer, V., Pal, S., Turner, D. D., and Wagner, E.: Can water vapour Raman lidar resolve profiles of turbulent variables in the convective boundary layer?, Bound.-Lay. Meteorol., 136, 253–284, 2010.